applied sciences

MDPI

Article

Torsional Behavior Evaluation of Reinforced Concrete Beams Using Artificial Neural Network

Muhammad Haroon [1,2], Seungbum Koo [3], DongIk Shin [1] and Changhyuk Kim [4,*]

1. School of Civil, Architectural Engineering and Landscape Architecture, Sungkyunkwan University, Seoul 03063, Korea; haroonbandija@gmail.com (M.H.); s91120@naver.com (D.S.)
2. Civil Engineering Balochistan UET, Khuzdar 89100, Pakistan
3. The MathWorks Inc., Natick, MA 01760, USA; findseungbum@gmail.com
4. Department of Architectural Engineering, Inha University, Incheon 22212, Korea

* Correspondence: changhyuk@inha.ac.kr; Tel.: +82-32-860-7565

Abstract: Artificial neural networks (ANNs) are an emerging field of research and have proven to have significant potential for use in structural engineering. In previous literature, many studies successfully utilized ANNs to analyze the structures under different loading conditions and verified the accuracy of the approach. Several studies investigated the use of ANNs to analyze the shear behavior of reinforced concrete (RC) members. However, few studies have focused on the potential use of an ANN for analysis of the torsional behavior of an RC member. Torsion is a complex problem and modeling the torsional fracture mechanism using the traditional analytical approach is problematic. Recent studies show that the nonlinear behavior of RC members under torsion can be modeled using ANNs. This paper presents a comprehensive analytical and parametric study of the torsional response of RC beams using ANNs. The ANN model was trained and validated against an experimental database of 159 RC beams reported in the literature. The results were compared with the predictions of design codes. The results show that ANNs can effectively model the torsional behavior of RC beams. The parametric study presented in this paper provides greater insight into the torsional resistance mechanism of RC beams and its characteristic parameters.

Keywords: RC beam; torsion; artificial neural network; machine learning; PCA; autoencoder

Citation: Haroon, M.; Koo, S.; Shin, D.; Kim, C. Torsional Behavior Evaluation of Reinforced Concrete Beams Using Artificial Neural Network. *Appl. Sci.* **2021**, *11*, 4465. https://doi.org/10.3390/app11104465

Received: 23 April 2021
Accepted: 11 May 2021
Published: 14 May 2021

1. Introduction

Most of the current design code [1–4] formulations for predicting the torsional response of reinforced concrete (RC) members are based on the space-truss model [5] and thin-walled tube theory [6]. However, due to the complex nature of the response of RC members to torque, these theories have undergone several developments and modifications, including the introduction of variable angle truss and bending phenomenon, compatibility equations, and softening of the concrete strut [7]. These developments are based on experimental observations and were introduced with the intent to develop a more uniform, rational, and easy-to-use behavior evaluation model. Torsion, which is a complicated three-dimensional problem, involves the equilibrium and compatibility of the whole 3D member [8]. Several design parameters, such as dimensions of the member, details of transverse and longitudinal reinforcement, and the strength of concrete, affect the torsional behavior of RC members. Extensive research studies have previously been carried out to investigate the effects of these variables on the torsional response of RC members. Hsu [9] presented an extensive experimental investigation of RC members under torsion with normal compressive strength of concrete. Victor and Muthukrishnan [10] investigated the effect of stirrups on the torque capacity of RC beams and developed an empirical equation for estimating the stirrup contribution to torque capacity. McMullen and Rangan [11] experimentally investigated the effect of the aspect ratio and amount of reinforcement on torsional strength of RC beams, and showed that the torsional strength decreases with an increase in aspect ratio. Collins and Mitchell [12] and Hsu and Mo [13] proposed compatibility aided analytical models capable of predicting the torsional behavior of RC members. Koutchoukali and Belarbi [14] and Fang and Shiau [15] experimentally studied the effect of high-strength concrete on the torsional behavior of RC beams. The studies showed that the high-strength concrete beams had higher torsional strength and cracking stiffness than the normal strength concrete beams. Chiu et al. [16] experimentally evaluated the torsional behavior of RC beams with minimum torsional reinforcement. They found that the post-cracking reserve strength in specimens with relatively low amounts of torsional reinforcement is primarily related to the transverse and longitudinal reinforcement ratio, in addition to the total amount of torsional reinforcement. Bernardo and Lopes [17] tested sixteen hollow high strength beams subjected to torsion and demonstrated that some design codes could lead to brittle torsional failure. Yang et al. [18] performed experiments to study the behavior of ultra-high performance concrete RC beams under torsion with a compressive strength greater than 150 MPa. Chalioris [19] and Chalioris and Karayannis [20] investigated the influence of the volume of stirrups, the location of longitudinal steel bars, and rectangular spiral reinforcement on the behavior of RC beams under torsion. A parametric study on torsional behavior of high strength concrete using nonlinear finite element analysis was also reported [21]. Recently, Lee et al. [22] examined the effect of maximum torsional reinforcement limitations specified in widely used design codes.

Despite these research efforts, a rational and easy-to-use torsional evaluation model has yet to be developed. This is due to (a) the complexities associated with the torsional behavior of RC members and (b) their testing limitations. Previous research has demonstrated that artificial neural networks (ANNs) can be an alternative approach for modeling of RC members under complex loading conditions. Several researchers have successfully employed ANNs to analyze the structures under different loading conditions and verified the accuracy of the approach by comparing it to the existing analytical methods. Previous research studies [23–32] investigated the potential use of ANNs to analyze the complex shear behavior of RC members and verified the existing design code formulation. These studies evaluated a variety of design parameters affecting the shear behavior of RC members with and without transverse reinforcement.

Because the current design codes perform a similar design process for the members under shear and torsional moment, an analytical approach for the shear can also be extended to analyze the torsional behavior. However, compared to studies of the shear, few research studies have utilized ANN models to analyze the torsional response of RC beams. Tang [33] used radial basis function neural networks (RBFNs) and Cevik et al. [34] utilized a genetic programming (GP) model to analyze the torsional strength of 76 RC beams and compared the results with design code equations. The results of these studies demonstrated that predicting the ultimate strength with RBFN and GP was feasible, and the prediction was better than existing code formulations. Similarly, Arslan [35] investigated the efficiency of different artificial neural networks in predicting the torsional strength of 76 RC beams. The study showed that each ANN model provides reasonable predictions of the ultimate torsional strength of RC beams.

It is evident from the literature that a large number of previous studies have focused on modeling the shear behavior of RC members using ANNs. However, The studies investigating torsional behavior are not only limited in number, but the databases used for training and validation of ANN models appear insufficient. Therefore, the potential use of ANNs in accurately modeling the torsional behavior of RC beams requires more detailed research with a more extensive test database for training and validation of the model. In this study, the torsional strength of RC beams was predicted using an ANN, and a parametric study of significant characteristic variables was carried out. The ANN model was trained and validated against a larger test database of 159 RC beams reported in the previous literature. A total of 10 main input variables were used to train the regression models. A back-propagation neural network (BPNN) was chosen to predict the torsional strength, and principal component analysis, in addition to autoencoder algorithms, were considered to improve the analysis results. The results of the ANN model were compared with the predictions of ACI 318-19, EC2-04, CSA-14, and JSCE-07.

2. Current Design Code Approaches for Torsion

2.1. ACI 318-19

The ACI 318-19 design provisions evaluate the maximum torsional strength of RC members based on a thin-walled tube space-truss analogy. The code suggests that after cracking, all the torsional actions are assumed to be resisted by stirrups and longitudinal reinforcement, without any concrete contribution. Therefore, in the calculation of Tn, only the torsional strength contribution from transverse and longitudinal reinforcement are considered, and the assistance from the concrete is ignored. According to the ACI 318-19 design code, the torsional resistance of non-prestressed and prestressed members shall be the lesser of (1) and (2):

$$T_n = \frac{2A_o A_t f_{ty}}{s} cot\theta \tag{1}$$

$$T_n = \frac{2A_o A_t f_y}{p_h} tan\theta \tag{2}$$

where θ shall not be taken to be less than 30° nor greater than 60°. A_t is the area of one leg of a closed stirrup resisting torsion, A_o is the area of longitudinal torsional reinforcement, $\boldsymbol{f_{ty}}$ and $\boldsymbol{f_y}$ are the yield strength of transverse and longitudinal torsional reinforcement, respectively, and p_h is the perimeter of the centerline of the outermost closed stirrup.

Once the torsional cracks are developed, the concrete outside of the stirrups becomes relatively ineffective. The total torsional stresses are carried by closed stirrups, longitudinal reinforcement, and concrete diagonals in compression. For this reason, A_o, the gross area enclosed by the shear flow path around the perimeter of the tube, is defined after cracking in terms of A_{oh}, the area enclosed by the centerline of the outermost closed transverse torsional reinforcement.

2.2. EC2-04

EC2-04 evaluates the maximum torsional strength of RC members based on the following equation:

$$T_{Rd,max} = 2v\alpha_{cw} f_{cd} A_k t_{ef,i} sin\theta cos\theta \tag{3}$$

Here, $T_{Rd,max}$ represents the maximum torsional resistance; v, the strength reduction factor for concrete cracked in shear; α_{cw}, coefficient taking account of the state of the stress in the compression chord of analogous truss; f_{cd}, the design value of concrete compressive strength; A_{k}, the area enclosed by the centerlines of the connecting walls *i* due to torque; $\boldsymbol{t_{ef,I}}$, the effective thickness of wall *i* due to torsion; θ, the strut angle.

2.3. CSA-14

Similar to ACI 318-19, CSA-14 utilizes the space-truss theory to compute the maximum torsional strength of RC members. The code suggests the following equation:

$$T_r = 2A_o \frac{\phi_s A_t f_y}{s} cot\theta \tag{4}$$

In this equation, $A_o = 0.85A_{oh}$ ($\boldsymbol{A_{oh}}$ is the area enclosed by the centerline of the exterior closed transverse torsion reinforcement, including area of holes (if any)). Although the basic equation for torsional resistance in CSA-14 is based on the concept of the space-truss analogy, the calculation of strut angle θ is somewhat different from that of the ACI 318-19 procedure. The θ in CSA-14 uses either a simplified method, in which θ should be taken to be equal to 35° when the yield strength of longitudinal steel reinforcement and specific compressive strength of concrete do not exceed 400 and 60 MPa, respectively; or a compatibility aided approach, in which θ is a function of axial strain at the mid-depth of the section ε_x. θ and ε_x can be calculated using Equations (5) and (6) as follows:

$$\theta = 29 + 7000\varepsilon_x \tag{5}$$

$$\varepsilon_x = \frac{M_f/d_v + V_f - V_p + 0.5N_f - A_p f_{po}}{2(E_s A_s + E_p A_p)}. \tag{6}$$

2.4. JSCE-07

JSCE-07 evaluates the maximum torsional strength of RC members based on the presence or absence of torsional reinforcement. The torsional capacity of members without torsional reinforcement can be calculated based on the elasticity theory using Equation (7), given below:

$$T_{tcd} = \beta_{nt} K_t \frac{f_{td}}{\gamma_b} \tag{7}$$

Here, T_{tcd} is the maximum torsional strength of members without torsional reinforcement and β_{nt} considers the effect of axial forces, such as prestressing forces. β_{nt} is taken as $\sqrt{1 + \sigma'_{nd}/(1.5f_{td})}$, where f_{td} is the tensile strength of concrete and σ'_{nd} is the average working compressive stress due to axial forces, which must be smaller than $7f_{td}$. The strength reduction factor γ_b is taken as 1.3 and the torsion factor K_t is calculated using the formula presented in Table 9.2.1 of the design code. K_t differs by the shape of the cross-section.

By comparison, the maximum torsional strength of members with torsional reinforcement can be evaluated using the Equation (8) (Equation 9.2.31 in JSCE-07 design code), which is based on the space-truss theory:

$$T_{tcd} = 2A_m \frac{\sqrt{q_w q_l}}{\gamma_b} \tag{8}$$

A_m in this equation is the effective area for torsion, which depends on the shape of the cross-section, and q_w and q_l are calculated as $A_{tw} f_{wd}/s$ and $\sum A_{tl} f_{ld}/u$, respectively. Here, A_{tl} and A_{tw} are the areas of longitudinal and single transverse reinforcement, respectively, that work effectively as torsion reinforcements, and $\boldsymbol{f_{ld}}$ and $\boldsymbol{f_{wd}}$ are their respective yielding strengths. s is the longitudinal spacing of transverse torsional reinforcement and u represents the length of centerline of transverse reinforcement, which is taken as $2(b_o+d_o)$ and πd_o for the rectangular and circular cross-sections, respectively.

3. Development of ANN Model

In this study, an ANN model for evaluating the ultimate torsional strength of RC beams was developed using the open-source software package WEKA3 [36]. The model utilizes the multilayer perceptron regression (MLP regression) algorithm. The theoretical details of MLP regression can be found in the work of Kim et al. [37]. Because the algorithm is well known and widely used for regression, the theoretical explanation is omitted in this paper. To improve and strengthen the accuracy of the ANN model, preprocessing algorithms were considered in this study. The algorithms used were principal component analysis and autoencoder, and the details of the algorithms are discussed in this section.

3.1. Data Selection for the Training and Validation Set

One of the most important elements in developing a neural network model is selection of the dataset, which is divided into two subsets: training data and testing data. Both stability and precision of the neural network model depend on the training phase [38,39]. In this research, a large experimental dataset of 159 specimens reported in the existing literature [9,11,14,15,22,40–43], was used for the training and validation of the ANN model. Almost 95% of the total data (151 specimens) was used for training and the remaining 5% (8 specimens) was used for validation. In this research, ten independent variables were used as input parameters for the ANN models. These input parameters include two sectional properties: width (b) and depth (h), both in millimeters; three variables related to closed stirrup: width (b'), depth (h'), and spacing (s), all in millimeters; the concrete compressive strength (f'_c), in MPa; and four reinforcement related properties: yield strength of the longitudinal reinforcement (f_{yl}) in MPa, longitudinal reinforcement ratio (ρ_l) in percent, yield strength of transverse reinforcement (f_{yt}) in MPa, and transverse reinforcement ratio (ρ_t) in percent. The output variable was set to be the maximum torsional strength ($T_{\max}$) of the RC beams. The sectional and material details of training and validation datasets are given in Appendix A Table A1. Before learning, the raw data was preprocessed for more efficient training and a better outcome.

3.2. Principal Component Analysis

Raw data $\boldsymbol{X^b} \in \mathbb{R}^{\boldsymbol{m}\times\boldsymbol{n}}$ used for training the learning algorithm in this article consisted of m = 151 experimental sequences, where each experimental sequence comprises n = 10 variables. Because each variable varies within different ranges for the datasets used in this article, they are typically normalized before being supplied for training. However, because not all variables are mutually independent, none of them are necessary for training nor they are in the best form (uncorrelated) for training the algorithm. PCA is a mathematical tool used to reduce the number of correlated variables in a dataset to uncorrelated variables called the principal components [44].

Finding the principal components of the given dataset $\boldsymbol{X^b}$ starts with column-wise normalization [45]:

$$X_i^a = \frac{X_i^b - \overline{X}_i^b 1}{\sigma\left(X_i^b\right)} \tag{9}$$

were X_i^b is the i–th column vectors of X^b, the over-bar indicates the mean of subtended term (therefore scalar), 1 is length–m column vector where all entries are unity, and $\sigma(X_i^b)$ represents the standard deviation of X_i^b. Performing this operation for all column vectors of X^b yields a column-wise normalized matrix X^a. The correlation matrix R^b, which is the table of correlation coefficients between all variables (columns) in the raw dataset, X^b, is equivalent to the covariance matrix of the column-wise normalized matrix X^a. The correlation coefficient r_{ij}^a between column vector i and j of X^b, namely X_i^b and X_j^b, is calculated as:

$$r_{ij}^a = \frac{1}{m-1}\frac{\left(X_i^b - \overline{X}_i^b 1\right)^T\left(X_i^b - \overline{X}_i^b 1\right)}{\sigma\left(X_i^b\right)\sigma\left(X_j^b\right)} \tag{10}$$

$$r_{ij}^a = \frac{1}{m-1}\left(X_i^a\right)^T X_j^a \tag{11}$$

Then, the correlation matrix R^b of X^a is simply the collection of $r_{ij}^a{}'$s as:

$$R^a = \begin{bmatrix} r_{11}^a & \cdots & r_{1n}^a \\ \vdots & \ddots & \vdots \\ r_{n1}^a & \cdots & r_{nn}^a \end{bmatrix} \tag{12}$$

To perform PCA, eigenvectors and eigenvalues of R^b are required. This is achieved by the eigenvalue decomposition as:

$$R^a = V^a \Lambda^a V^{aT} \tag{13}$$

where V^a is a matrix with the eigenvectors of R^b as its column vectors, and Λ^a is a diagonal matrix with the corresponding eigenvalues as its diagonal entries. Each eigenvector post-multiplied by the normalized data set X^a yields a principal component, and the significance of the computed principal component is represented by the corresponding eigenvalue, because it represents the variance of the designated principal component. The results are tabulated in Table 1.

$$X = X^a V^a \tag{14}$$

Table 1. Principal component results.

	PC1	PC2	PC3	PC4	PC5	PC6
b (mm)	0.448	−0.186	−0.117	0.307	−0.315	0.057
h (mm)	0.437	−0.089	−0.182	−0.396	0.229	0.075
b' (mm)	0.441	−0.133	−0.132	0.399	−0.340	0.086
h' (mm)	0.407	−0.101	−0.246	−0.440	0.271	0.230
f'_c (MPa)	−0.185	−0.416	−0.034	0.453	0.567	0.509
f_{yl} (MPa)	−0.060	−0.601	0.089	−0.055	−0.149	−0.242
ρ_l (%)	−0.362	−0.205	−0.330	−0.298	−0.239	0.203
f_{yt} (MPa)	−0.101	−0.585	0.119	−0.223	−0.145	−0.185
ρ_t (%)	−0.256	0.099	−0.557	−0.008	−0.370	0.364
s (mm)	0.060	0.024	0.658	−0.224	−0.316	0.637

Variables (columns) of the preprocessed dataset X are now linearly independent; that is, X is de-correlated. To determine if this is true, one may show that the correlation matrix of $X^T X$, namely R, is a diagonal matrix. Using Equations (10), (13), and (14) sequentially yields:

$$\begin{aligned} R = \tfrac{1}{m-1} X^T X = \tfrac{1}{m-1} (X^a V^a)^T X^a V^a = \tfrac{1}{m-1} (V^a)^T (X^a)^T X^a V^a = (V^a)^T R^a V^a \\ = (V^a)^T V^a \Lambda^a (V^a)^T V^a = I \Lambda^a I = \Lambda^a \end{aligned} \tag{15}$$

therefore, X is de-correlated.

When the column vectors of V^a are sorted in descending order regarding the corresponding eigenvalues before being multiplied, the resulting principal components in X are significant in the order they appear. Figure 1 shows the significance of each principal component for the dataset used in this article. The percentages are the normalized eigenvalues and their sum equals 100. As indicated, including the first six principal components is sufficient to represent 96% of the variance in the original data set X^b. We may choose these six principal components for training the learning algorithm and achieve a comparable prediction accuracy, and the dimensions of the input data set are reduced. In addition, the quality of the data set is improved because the principal components are linearly independent.

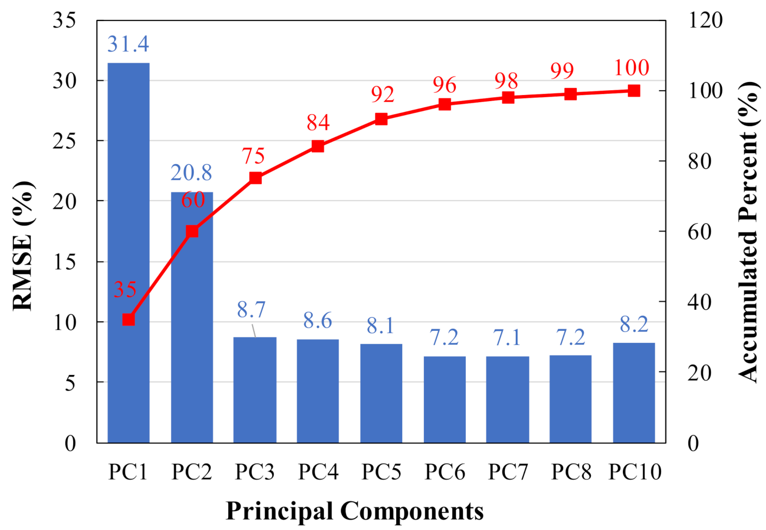

Figure 1. Significance of each principal component.

3.3. Autoencoder

Dimension reduction, or feature extraction in machine learning terminology, particularly in image analysis applications, is also possible using the method called autoencoding, which is an unsupervised learning technique using an ANN. Autoencoder uses the (normalized) raw data as input and output at the same time. To benefit from the dimension reduction, the classical autoencoder sets the number of nodes in the hidden layer intentionally less than the input layer dimension [46]. A typical neural network architecture of an autoencoder with fewer hidden layer nodes than in the input is shown in Figure 2. Autoencoder takes the raw data X^b from the input layer and predicts the output $\hat{X}^b$ such that X and $\hat{X}^b$ are close. Because the data goes through a hidden layer, which has fewer nodes than the number of nodes in the input layer, the autoencoder tries to squeeze the information in the input to fit into the hidden layer. This process in called encoding. After the compression, the autoencoder decodes the data to reconstruct the input. When the autoencoder finds a way to successfully reconstruct the data $\hat{X}^b$, which is close enough to the input X^b, we can conclude that the squeezed information in the hidden layer has sufficient information to closely describe the original data X^b but with a reduced dimension. We refer to the compressed data as code. Because the code is considered to have sufficient information to describe the raw data, using the code for training the learning algorithm would be (almost) equivalent to training using the original data, and the dimension of the data is reduced, as in PCA.

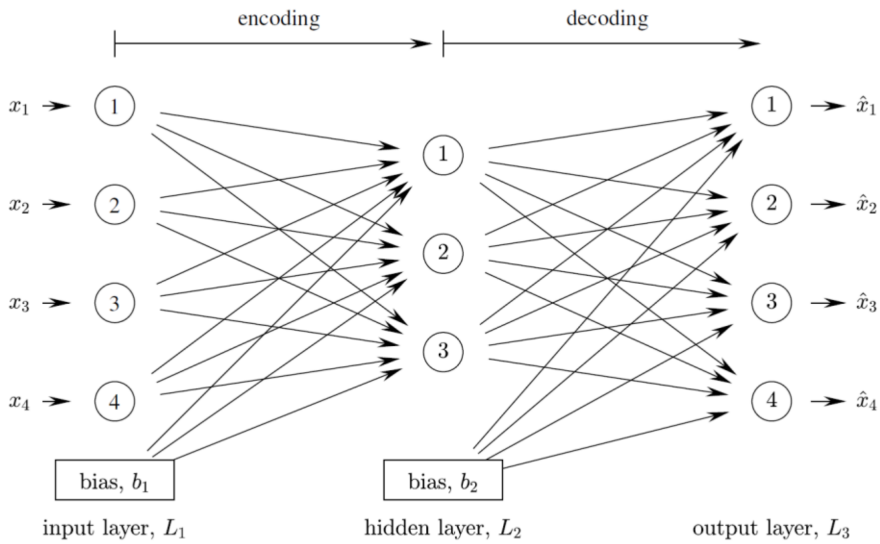

Figure 2. Simplified typical neural network architecture to implement an autoencoder.

A similar benefit, however, can be achieved by setting the number of nodes in the hidden layer to be greater than in the input with sparsity constraints [47–49]; this allows a greater number of hidden layer nodes than in the input layer, of which only a few are activated, while most of the nodes remain inactive. Such an autoencoder is called the sparse autoencoder and is known to have the advantage that, by using a dimension higher than the original data, the likelihood that each experimental datapoint is easily distinguishable is increased [50]. In this article, we used this sparse autoencoder with one hidden layer consisting of 20 units (whereas the original data had 10 variables). The coded data was then fed into the learning algorithm with one hidden layer with 24 nodes for training.

3.4. Results of ANN Analysis

To develop the regression models, one layer of the hidden layer and two different preprocessing filters were applied to the ANN models. A total number of 52 and 24 hidden nodes were selected for the ANN models with two preprocessing algorithms: PCA and autoencoder. The number of hidden nodes was chosen based on the trial-and-error method. The activation function for the models was a sigmoid function. The calculated weight values between the input-to-hidden layers and hidden-to-output layers are summarized in Tables A2 and A3 for PCA and autoencoder, respectively.

The maximum torsional strength of 151 specimens of the training dataset was predicted using the ANN models developed in this study and compared with the predictions of the most widely used design codes. Figure 3 shows comparison plots between the experimental results and the calculated torsional strength of specimens. The x-axis represents the measured torsional strength of specimens and the y-axis presents the predicted torsional strength by the design codes and developed ANN models. As shown in the figure, among the four design codes, ACI 318-19 (Figure 3a) showed better predictions with mean value and coefficient of variation (CV) of 0.98 and 25.18%, respectively. CSA-14 (Figure 3c) and JSCE-07 (Figure 3d) overestimated the maximum torsional strength of RC beams. The mean value of the ratio of experimental torsional strength to predicted torsional strength using CSA-14 was 0.71 with a CV of 25.18%, and the mean and CV for JSCE-07 were 0.86 and 23.46%, respectively. EC2-04 (Figure 3b) mainly underestimated the maximum torsional strength of RC beams. The mean and CV obtained using EC2-04 were 1.14 and 29.36%, respectively. In contrast, the ANN models successfully predicted the maximum torsional strength of RC beams with the best mean and CV, compared to the four design codes. The ANN model with two preprocessors—PCA (Figure 3e) and autoencoder (Figure 3f)—resulted in a mean value of 1.0 for the ratio of experimental to predicted torsional strength. The CV with PCA and autoencoder was 5.47% and 2.86%, respectively, which is significantly lower than the CV of design code predictions.

The accuracy of the analysis results using current design codes and the developed ANN algorithms was further evaluated based on three different errors: Root Mean Square Error (RMSE), Relative Absolute Error (RAE), and Root Relative Square Error (RRSE). Table 2 summarizes the calculated correlation coefficients and error percentages. The correlation coefficient of the developed ANN algorithms was 0.9968 and 0.9993 for PCA and autoencoder, respectively. The results from the developed ANN models well reflected the training data set, and significantly lower error percentages were obtained by utilizing the developed ANN models. All the calculated errors of the ANN models were lower than 10%.

Table 2. Prediction accuracies.

	ACI 318-19	EC2-04	CSA-14	JSCE-07	PCA	Autoencoder
Correlation Coefficient	0.9369	0.9467	0.8924	0.9260	0.9968	0.9993
Root Mean Square Error	16.1713	14.4432	36.8951	22.8708	3.4492	1.6022
Relative Absolute Error	32.1298	30.9552	76.4643	42.4559	6.5440	2.9346
Root Relative Square Error Error (%)	37.6681	33.6429	85.9407	53.2735	8.0344	3.7321

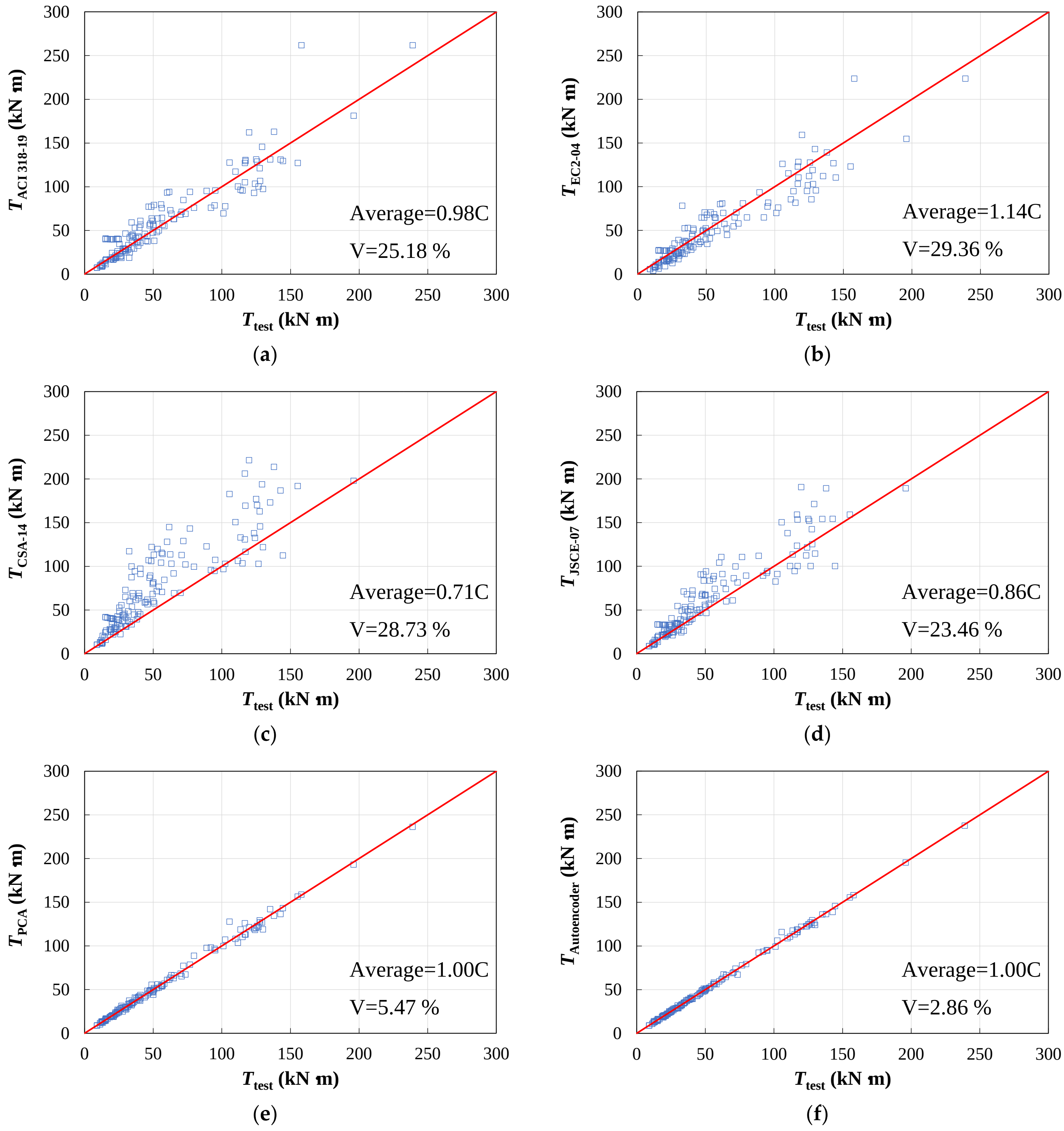

Figure 3. Comparisons between predicted and measured torsional strength of the training dataset. (**a**) ACI 318-19; (**b**) EC2-04; (**c**) CSA-14; (**d**) JSCE-07; (**e**) PCA; (**f**) autoencoder.

4. Model Validation

4.1. Validation Data Set

After the analysis of training dataset, the proposed ANN model was validated against a dataset of eight RC beams subjected to torsional moments. These eight specimens were not used for the training set. Details of the specimens and test results are summarized in Table 3. Because eight specimens were extracted from five different experimental test programs, the details of each specimen were different.

Table 3. Details of the validation set specimens.

Specimen	Section Details				Concrete	Longitudinal Bar		Transverse Bar		Test Strength
	b (mm)	h (mm)	b' (mm)	h' (mm)	f_c' (MPa)	ρ_l (%)	f_{yl} (MPa)	ρ_t (%)	f_{yt} (MPa)	s (mm)	T_u (kN·m)
B-1	300	350	247	29	42.2	1.00	659	1.01	667	130	47.64
B-2	300	350	247	297	68.4	1.51	310	1.88	340	70	66.71
B-3	320	370	247	297	26.0	0.86	353	0.90	353	130	34.91
B-4	320	370	247	297	50.0	0.43	480	0.53	480	220	34.05
B-5	400	600	310	510	35.3	0.93	320	0.93	334	53	126.11
B-6	400	600	310	510	35.3	0.69	309	0.67	334	73	110.14
B-7	203	305	165	267	93.9	0.82	386	0.92	386	108	21.00
B-8	254	508	216	470	30.9	0.62	323	0.63	334	121	40.34

4.2. Validation Data Results

The maximum torsional strength of the specimens was calculated using the ANN algorithms with two preprocessors, PCA and autoencoder, and current four design codes. In Figure 4, the validation results of the algorithms were compared with the prediction of design codes. The *x*-axis represents the specimen name and the *y*-axis shows the ratio of the test to calculated torsional strength. In Figure 4a, the circular, diamond, triangular, and cross markers represent ACI 318-19, EC2-04, CSA-14, and JSCE-07, respectively, whereas in Figure 4b, the circular and cross markers indicate the ANN algorithm results with PCA and autoencoder, respectively. The mean value, standard deviation, and CV of the validation set are presented in Table 4. As shown in Figure 4 and Table 4, the ANN model accurately predicted the maximum torsional strength compared to the predictions of design codes, even if the models were untrained for this data set. The ANN models resulted in the best mean and CV values of 0.96 and 2.27%, respectively, for PCA, and 1.05 and 11.55%, respectively, for the autoencoder. In contrast, ACI 318-19 and EC2-04 overestimated, and JSCE-07 and CSA-14 mainly underestimated, the maximum torsional strength of RC beams. The mean and CV values for ACI 318-19, EC2-04, CSA-14, and JSCE-07 were 1.09, 1.13, 0.701, 0.88 and 22.32%, 22.95%, 23.57%, 21.55%, respectively.

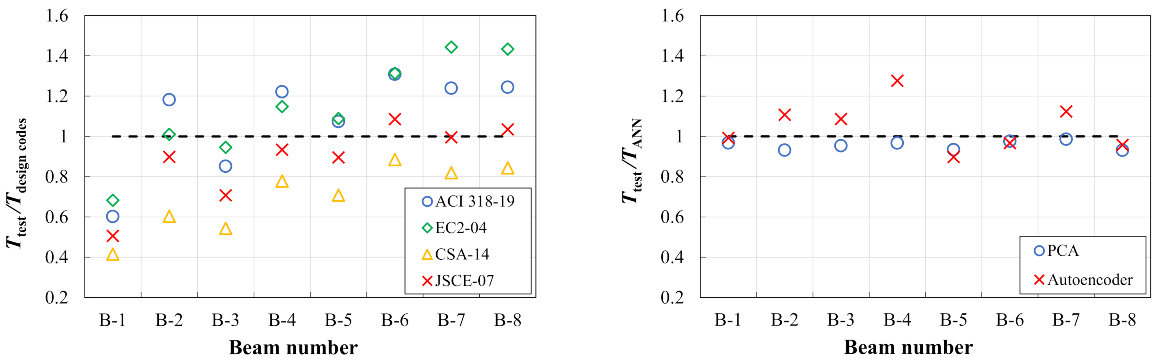

(**a**) (**b**)

Figure 4. Comparisons between predicted and measured torsional strength of the validation dataset. (**a**) Current design codes; (**b**) ANN models.

Table 4. Statistical values of the validation dataset.

	ACI 318-19	EC2-04	CSA-14	JSCE-07	PCA	Autoencoder
Mean	1.09	1.13	0.70	0.88	0.96	1.05
Standard deviation	0.24	0.26	0.16	0.19	0.02	0.12
Coefficient of variation	22.32	22.95	23.57	21.55	2.27	11.55

5. Parametric Study

A parametric study was conducted to evaluate the potential effects of input variables on the torsional strength of RC beams. RC beam H1-540-100 from the training dataset in Table A1 was chosen as a reference beam for this parametric study. To investigate the effect of an individual variable on torsional strength, all the other variables were fixed while the individual variable was varied. Figures 5 and 6 show the results of the parametric study of 10 variables using the ANN with PCA and autoencoder, respectively. The *x*-axis represents the range of the individual variable and the *y*-axis indicates the normalized torsional strength in MPa. The empty square markers represent the experimental test data. The double-lined curves in Figures 5 and 6 are the trained ANN models with PCA and autoencoder algorithms, respectively. The solid, dotted, dashed, and dash-dot curves are the calculated normalized torsional strength from ACI 318-19, EC2-04, CSA-14, and JSCE-07, respectively.

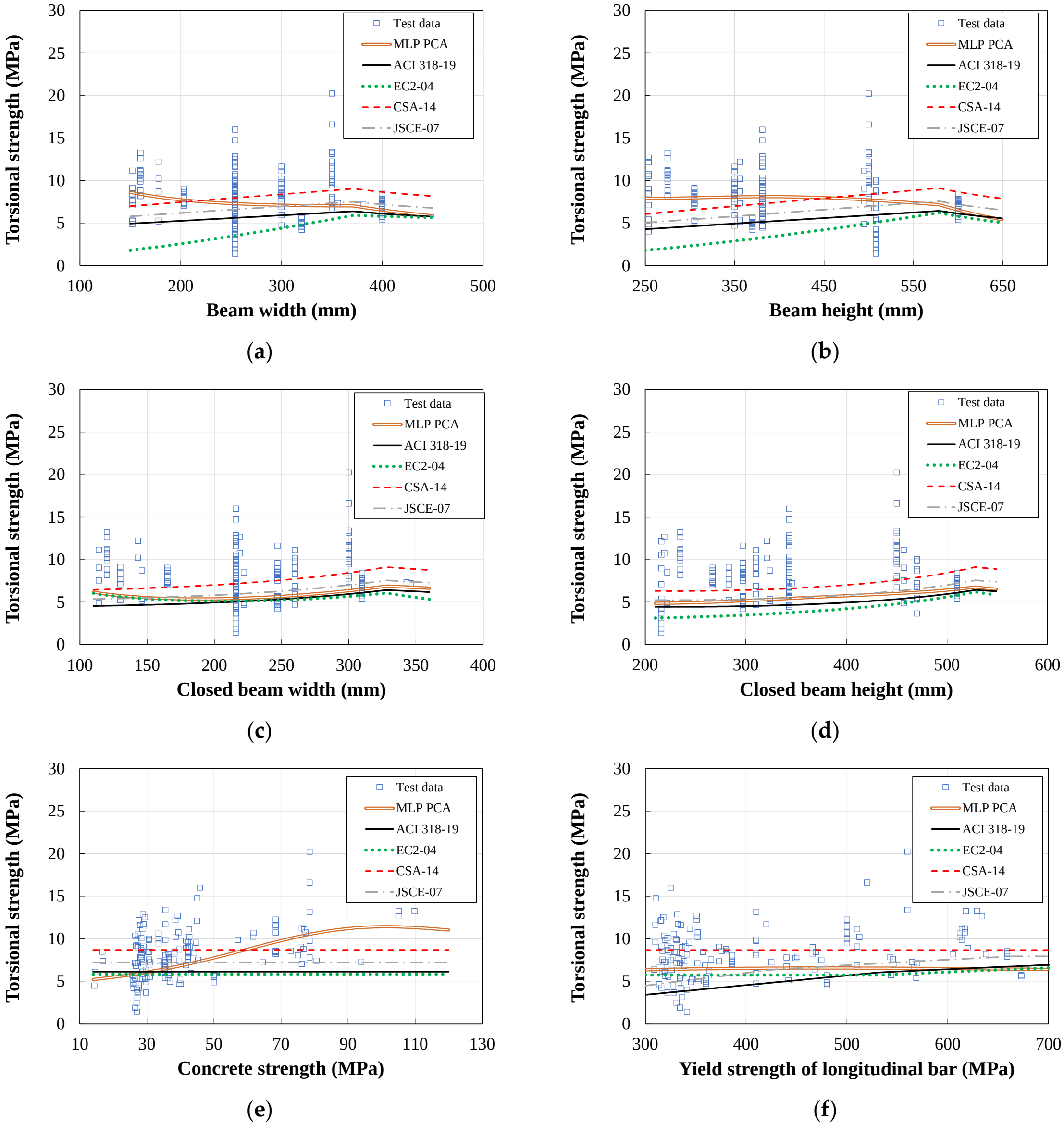

Figure 5. *Cont.*

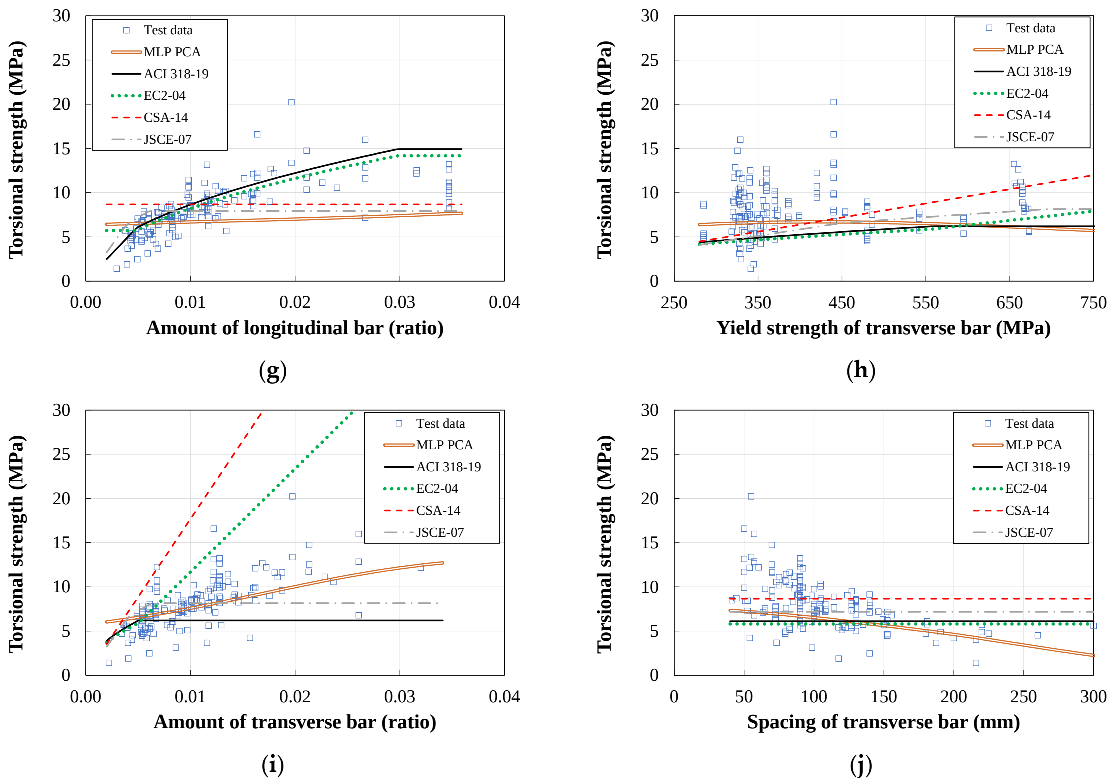

Figure 5. Parametric study using PCA: (**a**) beam width; (**b**) beam height; (**c**) closed beam width; (**d**) closed beam height; (**e**) concrete strength; (**f**) yield strength of longitudinal bar; (**g**) amount of longitudinal bar; (**h**) yield strength of transverse bar; (**i**) amount of transverse bar; (**j**) spacing of transverse bar.

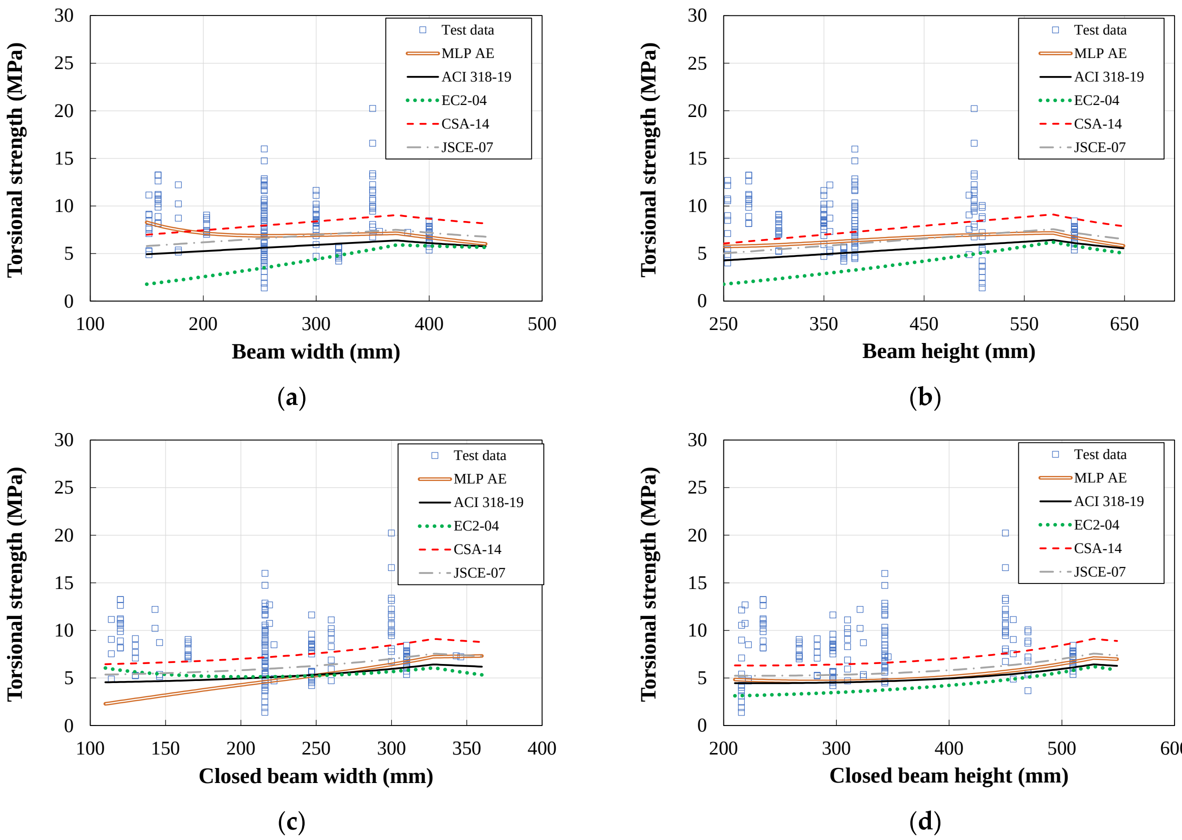

Figure 6. *Cont.*

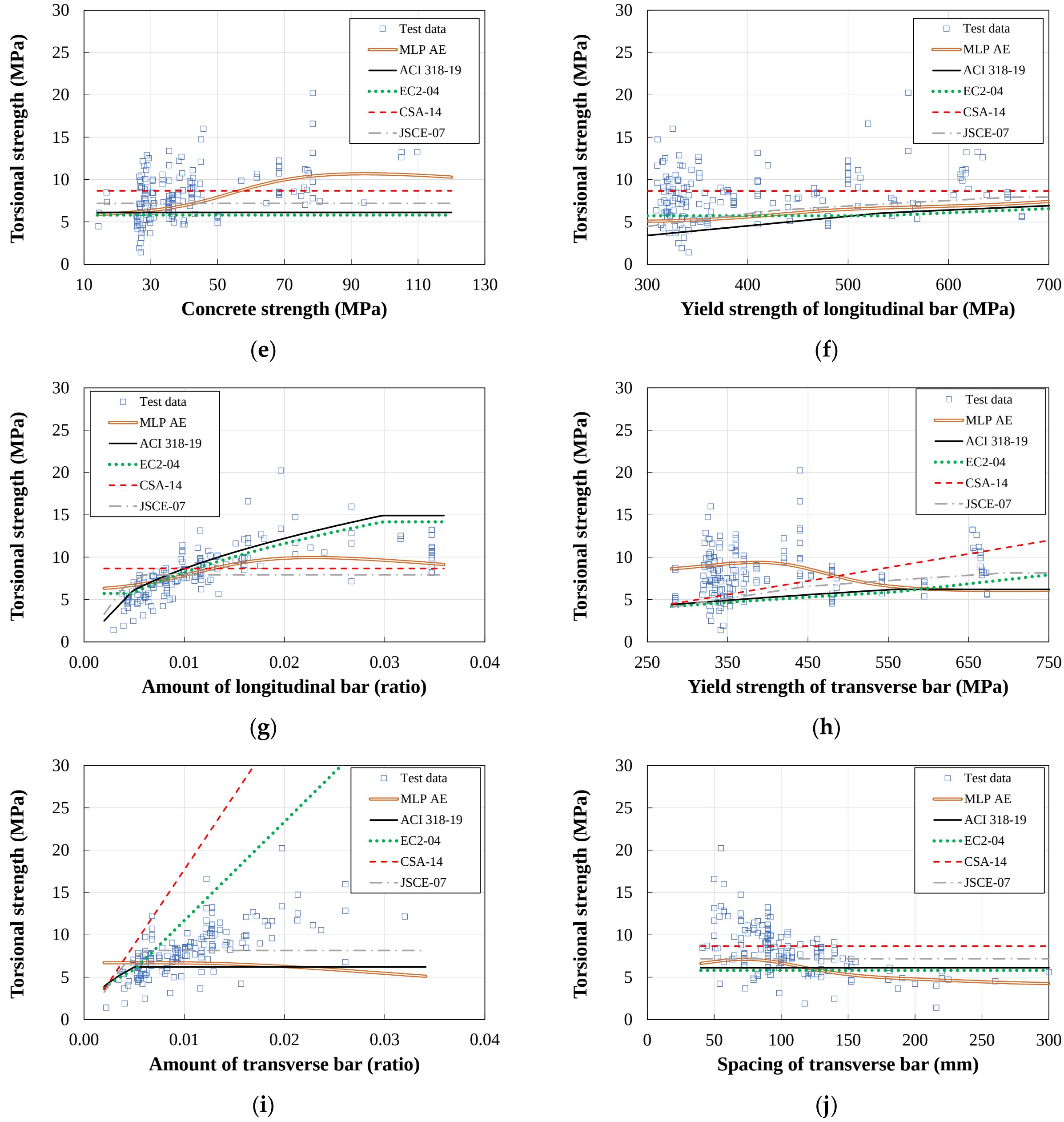

Figure 6. Parametric study using autoencoder: (**a**) beam width; (**b**) beam height; (**c**) closed beam width; (**d**) closed beam height; (**e**) concrete strength; (**f**) yield strength of longitudinal bar; (**g**) amount of longitudinal bar; (**h**) yield strength of transverse bar; (**i**) amount of transverse bar; (**j**) spacing of transverse bar.

5.1. Size of Concrete Section

Figures 5 and 6a–d show the results of the analysis of the cross-sectional size effect on torsional strength of RC beams. The size effect of the concrete cross-section and closed section was nearly negligible among the test results. No clear trend was observed in the experimental data with increasing beam section width and overall depth; nor did the ANN model show any significant variation in torsional strength. The figures show a large scattering without an obvious tendency, which implies that the other input variables affect the torsional strength of RC beams more than the sectional dimensions and size.

5.2. Concrete Strength

Although the current design codes neglect the contribution of concrete to the torsional strength of RC members, the experimental results show the increasing torsional strength with increasing compressive strength of concrete. As shown in Figures 5 and 6e, the ANN with PCA and autoencoder can effectively take into consideration the effect of concrete compressive strength. The calculated torsional strength with ANN tends to increase as the concrete strength increases, whereas the design codes predict no effect of concrete strength on the torsional strength of RC beams.

5.3. Amount and Yielding Strength of Longitudinal Reinforcement

The analysis results in Figures 5 and 6f–g show that the yield strength of longitudinal reinforcement does not significantly affect the torsional behavior. The torsional behavior is rather more affected by the amount of longitudinal reinforcement than its yield strength. As shown in the figure, the torsional strength remained nearly the same for all ranges of yielding strengths, which was effectively represented by the current design codes and the ANN algorithms. However, the torsional strength increased as the amount of longitudinal reinforcement increased. This increasing trend of torsional strength was well reflected by ACI 318-19 and EC2-04 design codes.

5.4. Amount and Yielding Strength of Transverse Reinforcement

The effect of the transverse reinforcement was nearly the same as the effect of the longitudinal reinforcement. Figures 5 and 6h–j represent the effect of yielding strength, amount, and spacing of transverse reinforcement on torsional strength of RC beams. A slightly increasing trend of the torsional strength was observed with the increasing yield strength of transverse reinforcement. This effect was well accounted for in all design codes. In the case of the amount of transverse reinforcement, EC2-04 and CSA-14 overestimated the torsional strength of RC beams. The ANN algorithms well predicted the increasing trend of the torsional strength with increasing amount of transverse reinforcement. Spacing of transverse reinforcement was reflected by the amount of transverse reinforcement. Therefore, an independent effect of the spacing of transverse reinforcement on torsional strength cannot clearly be observed by the current design codes.

6. Conclusions

In this research, a back-propagation neural network (BPNN) model was used to predict the ultimate torsional strength of RC beams. A total of 159 experimental datapoints were collected from previous experimental test programs to train and validate ANN models. Before training, the raw data was preprocessed using principal component analysis (PCA) and the sparse autoencoder technique to enhance the quality of the training dataset. The analysis results obtained using the ANN model were compared with the predictions of four design codes. Significant results were obtained, as follows:

- The data collected to utilize the ANN technique was almost double that of the existing publications.
- In addition to BPNN algorithms, two preconditioners, PCA and an autoencoder, were also used. These were shown to increase the accuracy.
- Predicting the torsional strength of RC beams was straightforward with the trained ANN algorithms.
- The trained ANN could better reflect the effect of input variables for those that were not well reflected by the current design codes.

A parametric study was conducted to evaluate the potential effect of each input variable on the torsional behavior of RC beams. First, the cross-sectional size effect and the enclosed section size effect were not observed. The torsional strength of the RC beams did not show any noticeable change per the change in the concrete size-related variables. Second, the concrete compressive strength showed a positive relationship to the torsional strength, which was capped around 90 MPa. Third, the amount of longitudinal reinforcement positively affected the torsional strength, whereas the contribution of yield strength was less significant. Finally, similar trends were observed from the transverse reinforcement-related variables, in terms of effective amount and less-effective yield strength. A decrease in torsional strength was observed as the spacing increased.

Author Contributions: M.H. and C.K. accumulated the experimental data, conducted analysis and wrote the manuscript. S.K. provided assistance in ANN model development and validation. D.S. reviewed the manuscript and provided useful technical assistance. All authors have read and agreed to the published version of the manuscript.

Funding: This research received no external funding.

Institutional Review Board Statement: This research received no external funding.

Informed Consent Statement: Not applicable.

Data Availability Statement: All the research data used in this manuscript will be available whenever requested.

Conflicts of Interest: The authors declare no conflict of interest.

Appendix A

Table A1. Details of the Training Set Data.

Specimen	Section Details				Concrete	Longitudinal Bar		Transverse Bar			Test Strength
	b (mm)	h (mm)	b' (mm)	h' (mm)	f_c'(MPa)	ρ_l (%)	f_{yl} (MPa)	ρ_t (%)	f_{yt} (MPa)	s (mm)	T_u (kNm)
T1-C42S40	300	350	247	297	42.2	1.00	317	1.01	340	130	44.62
T1-C42S50	300	350	247	297	42.2	1.00	469	1.01	480	130	50.06
T1-C70S40	300	350	247	297	68.4	1.00	317	1.01	340	130	50.79
T1-C70S50	300	350	247	297	68.4	1.00	469	1.01	480	130	50.06
T1-C70S60	300	350	247	297	68.4	1.00	659	1.01	667	130	50.45
T2-C42S40	300	350	247	297	42.2	1.51	310	1.88	340	70	56.83
T2-C42S50	300	350	247	297	42.2	1.13	466	1.46	480	90	53.21
T2-C42S60	300	350	247	297	42.2	1.00	659	0.94	667	140	46.65
T2-C70S50	300	350	247	297	68.4	1.13	466	1.46	480	90	48.86
T2-C70S60	300	350	247	297	68.4	1.00	659	0.94	667	140	48.55
C24SD30-ACI	320	370	247	297	26.0	0.67	335	0.58	353	200	30.16
C24SD30-EC	320	370	247	297	26.0	1.34	335	1.29	353	90	40.60
C24G60-ACI	320	370	247	297	26.0	0.43	480	0.45	480	260	31.58
C24G60-mid	320	370	247	297	26.0	0.64	480	0.65	480	180	32.80
C24G60-EC	320	370	247	297	26.0	0.88	442	0.97	480	120	36.64
C42G60-mid	320	370	247	297	50.0	0.64	480	0.78	480	150	39.70
C42G80-ACI	320	370	247	297	50.0	0.43	673	0.39	673	300	38.96
C42G80-mid	320	370	247	297	50.0	0.64	673	0.53	673	220	39.83
T1-350-65	400	600	310	510	35.4	0.75	313	0.75	334	65	123.45
T1-480-90	400	600	310	510	35.4	0.55	475	0.54	486	90	124.11
T1-660-122.5	400	600	310	510	35.4	0.44	569	0.40	595	123	88.87
T2-480-72.5	400	600	310	510	35.3	0.69	468	0.67	486	73	105.61

Table A1. *Cont.*

Specimen	Section Details				Concrete	Longitudinal Bar		Transverse Bar			Test Strength
	b (mm)	h (mm)	b' (mm)	h' (mm)	f'_c(MPa)	ρ_l (%)	f_{yl} (MPa)	ρ_t (%)	f_{yt} (MPa)	s (mm)	T_u (kNm)
T2-660-100	400	600	310	510	35.3	0.54	567	0.49	595	100	109.91
T3-350-90	400	600	310	510	35.4	0.55	318	0.54	334	90	101.10
T3-660-90	400	600	310	510	35.4	0.60	570	0.54	595	90	117.15
T4-660-72.5	400	600	310	510	35.3	0.75	565	0.67	595	73	119.83
H1-350-65	400	600	310	510	36.5	0.75	365	0.75	356	65	127.83
H1-480-90	400	600	310	510	36.5	0.55	451	0.54	454	90	129.92
H1-540-100	400	600	310	510	36.5	0.50	546	0.49	542	100	116.80
H2-350-52.5	400	600	310	510	30.7	0.93	357	0.93	360	53	142.81
H2-480-72.5	400	600	310	510	36.5	0.69	449	0.67	454	73	127.54
H2-540-80	400	600	310	510	36.5	0.60	545	0.61	542	80	125.65
H3-350-90	400	600	310	510	36.5	0.55	363	0.54	356	90	102.48
H3-540-135	400	600	310	510	36.5	0.38	544	0.36	542	135	94.71
H4-350-72.5	400	600	310	510	30.7	0.69	359	0.67	360	73	113.65
H4-540-72.5	400	600	310	510	36.5	0.69	543	0.67	542	73	129.32
B5UR1	203	305	165	267	39.6	0.82	386	0.92	373	108	19.40
B7UR1	203	305	165	267	64.6	0.82	386	0.92	399	108	18.90
B9UR1	203	305	165	267	75.0	0.82	386	0.92	373	108	21.10
B12UR1	203	305	165	267	80.6	0.82	386	0.92	399	108	19.40
B12UR2	203	305	165	267	76.2	0.82	386	0.97	386	102	18.40
B12UR3	203	305	165	267	72.9	1.05	376	1.04	386	95	22.50
B12UR4	203	305	165	267	75.9	1.23	373	1.10	386	90	23.70
B12UR5	203	305	165	267	76.7	1.28	380	1.41	386	70	24.00
B1	254	381	216	343	27.6	0.53	314	0.54	341	152	22.26
B2	254	381	216	343	28.6	0.83	316	0.82	320	181	29.26
B3	254	381	216	343	28.1	1.17	328	1.17	320	127	37.51
B4	254	381	216	343	30.5	1.60	320	1.62	323	92	47.34
B5	254	381	216	343	29.0	2.11	332	2.13	321	70	56.16
B6	254	381	216	343	28.8	2.67	332	2.61	323	57	61.69
B7	254	381	216	343	26.0	0.53	320	1.17	319	127	26.89
B8	254	381	216	343	26.8	0.53	322	2.61	320	57	32.54
B9	254	381	216	343	28.8	1.17	319	0.54	343	152	29.83
B10	254	381	216	343	26.5	2.67	334	0.54	342	152	34.35
D1	254	381	216	343	26.6	0.53	333	0.54	338	152	22.37
D2	254	381	216	343	25.6	0.83	323	0.82	331	181	27.68
D3	254	381	216	343	28.4	1.17	341	1.17	333	127	39.09
D4	254	381	216	343	30.6	1.60	330	1.62	333	92	47.91
M1	254	381	216	343	29.9	0.83	326	0.55	353	149	30.39
M2	254	381	216	343	30.5	1.17	329	0.78	357	105	40.56

Table A1. *Cont.*

Specimen	Section Details				Concrete	Longitudinal Bar		Transverse Bar			Test Strength
	b (mm)	h (mm)	b' (mm)	h' (mm)	f'_c(MPa)	ρ_l (%)	f_{yl} (MPa)	ρ_t (%)	f_{yt} (MPa)	s (mm)	T_u (kNm)
M3	254	381	216	343	26.8	1.60	322	1.07	326	140	43.84
M4	254	381	216	343	26.5	2.11	319	1.42	327	105	49.60
M5	254	381	216	343	28.0	2.67	335	1.81	331	83	55.70
M6	254	381	216	343	29.4	3.16	318	2.13	341	70	60.11
I2	254	381	216	343	45.2	0.83	325	0.83	349	98	36.04
I3	254	381	216	343	44.7	1.17	343	1.17	334	127	45.65
I4	254	381	216	343	45.0	1.60	315	1.62	326	92	58.08
I5	254	381	216	343	45.0	2.11	310	2.13	325	70	70.73
I6	254	381	216	343	45.8	2.67	325	2.61	329	57	76.72
G1	254	508	216	470	29.8	0.40	322	0.40	339	187	26.78
G3	254	508	216	470	26.8	0.88	339	0.88	328	156	49.60
G4	254	508	216	470	28.3	1.20	325	1.20	321	114	64.86
G5	254	508	216	470	26.9	1.58	331	1.60	328	86	71.98
G6	254	508	216	470	29.9	0.60	334	0.59	350	127	39.09
G7	254	508	216	470	31.0	0.93	319	0.94	323	146	52.65
G8	254	508	216	470	28.3	1.32	322	1.31	329	105	73.45
N1	152	305	130	283	29.5	0.61	352	0.61	341	92	9.09
N1A	152	305	130	283	28.7	0.61	346	0.61	345	92	8.99
N2	152	305	130	283	30.4	1.11	331	1.11	338	51	14.46
N2A	152	305	130	283	28.4	1.11	333	1.11	361	114	13.22
N3	152	305	130	283	27.3	0.91	352	0.89	352	64	12.20
N4	152	305	130	283	27.3	1.42	340	1.42	356	89	15.70
K1	152	495	114	457	29.9	0.56	345	0.57	354	191	15.36
K2	152	495	114	457	30.6	1.02	336	1.03	338	105	23.73
K3	152	495	114	457	29.0	1.59	316	1.58	321	124	28.47
K4	152	495	114	457	28.6	2.26	344	2.28	340	86	35.03
C1	254	254	216	216	27.0	0.44	341	0.44	341	216	11.30
C2	254	254	216	216	26.5	0.80	334	0.81	345	117	15.25
C3	254	254	216	216	26.9	1.24	331	1.24	330	140	20.00
C4	254	254	216	216	27.2	1.76	336	1.76	328	98	25.31
C5	254	254	216	216	27.2	2.40	328	2.37	329	73	29.71
C6	254	254	216	216	27.6	3.16	316	3.20	328	54	34.23
J1	254	381	216	343	14.3	0.53	328	0.54	346	152	21.47
J2	254	381	216	343	14.5	0.83	320	0.83	341	98	29.15
J3	254	381	216	343	16.9	1.17	339	1.17	337	127	35.25
J4	254	381	216	343	16.8	1.60	324	1.62	332	92	40.68
PT4	381	381	346	346	28.6	1.10	425	0.66	328	102	70.00

Table A1. *Cont.*

Specimen	Section Details				Concrete	Longitudinal Bar		Transverse Bar			Test Strength
	b (mm)	h (mm)	b' (mm)	h' (mm)	f'_c(MPa)	ρ_l (%)	f_{yl} (MPa)	ρ_t (%)	f_{yt} (MPa)	s (mm)	T_u (kNm)
PT5	356	356	343	343	33.8	1.26	373	0.75	328	102	65.20
A1	254	254	222	222	36.9	0.44	360	0.55	285	79	13.10
A1R	254	254	222	222	39.6	0.44	360	0.55	285	79	12.50
A2	254	254	222	222	38.2	0.80	380	1.06	285	41	22.60
A3	254	254	219	219	39.4	1.24	352	1.21	360	79	27.80
A4	254	254	219	219	39.2	1.77	351	1.69	360	57	34.50
B1	178	356	146	324	36.3	0.45	360	0.57	285	83	12.80
B1R	178	356	146	324	39.9	0.45	360	0.57	285	83	12.30
B2	178	356	146	324	39.6	0.81	380	1.06	285	44	20.80
B3	178	356	143	321	38.6	1.26	352	1.26	360	83	25.30
B4	178	356	143	321	38.5	1.80	351	1.72	360	60	31.80
B30.1	160	275	120	235	41.7	3.47	620	1.28	665	90	16.62
B30.2	160	275	120	235	38.2	3.47	638	1.28	669	90	15.29
B30.3	160	275	120	235	36.3	3.47	605	1.28	672	90	15.25
B50.1	160	275	120	235	61.8	3.47	612	1.28	665	90	19.95
B50.2	160	275	120	235	57.1	3.47	614	1.28	665	90	18.46
B50.3	160	275	120	235	61.7	3.47	612	1.28	665	90	19.13
B70.1	160	275	120	235	77.3	3.47	617	1.28	658	90	20.06
B70.2	160	275	120	235	76.9	3.47	614	1.28	656	90	20.74
B70.3	160	275	120	235	76.2	3.47	617	1.28	663	90	20.96
B110.1	160	275	120	235	109.8	3.47	618	1.28	655	90	24.72
B110.2	160	275	120	235	105.0	3.47	634	1.28	660	90	23.62
B110.3	160	275	120	235	105.1	3.47	629	1.28	655	90	24.77
T1-1	300	350	260	310	43.2	0.48	410	0.60	370	130	32.86
T1-2	300	350	260	310	44.0	0.72	410	0.91	370	85	45.89
T1-3	300	350	260	310	41.7	0.97	410	1.19	370	65	54.05
T1-4	300	350	260	310	42.6	1.13	510	1.83	355	75	62.41
T2-1	300	350	260	310	40.1	0.48	410	0.34	370	225	26.05
T2-2	300	350	260	310	41.7	0.76	510	0.60	370	130	38.11
T2-3	300	350	260	310	42.7	1.13	510	0.88	370	88	50.16
T2-4	300	350	260	310	42.6	1.33	512	1.03	370	75	56.39
H-06-06	350	500	300	450	78.5	0.68	440	0.61	440	100	92.00
H-06-12	350	500	300	450	78.5	1.16	410	0.61	440	100	115.10
H-12-12	350	500	300	450	78.5	1.16	410	1.22	440	50	155.30
H-12-16	350	500	300	450	78.5	1.64	520	1.22	440	50	196.00
H-20-20	350	500	300	450	78.5	1.96	560	1.97	440	55	239.00
H-07-10	350	500	300	450	68.4	0.98	500	0.68	420	90	126.70
H-14-10	350	500	300	450	68.4	0.98	500	1.36	360	80	135.20
H-07-16	350	500	300	450	68.4	1.64	500	0.68	420	90	144.50

Table A1. *Cont.*

Specimen	Section Details				Concrete	Longitudinal Bar		Transverse Bar			Test Strength
	b (mm)	h (mm)	b' (mm)	h' (mm)	f'_c(MPa)	ρ_l (%)	f_{yl} (MPa)	ρ_t (%)	f_{yt} (MPa)	s (mm)	T_u (kNm)
N-06-06	350	500	300	450	35.5	0.68	440	0.61	440	100	79.70
N-06-12	350	500	300	450	35.5	1.16	410	0.61	440	100	95.20
N-12-12	350	500	300	450	35.5	1.16	410	1.22	440	50	116.80
N-12-16	350	500	300	450	35.5	1.64	420	1.22	440	50	138.00
N-20-20	350	500	300	450	35.5	1.96	560	1.97	440	55	158.00
N-07-10	350	500	300	450	33.5	0.98	500	0.68	420	90	111.70
N-14-10	350	500	300	450	33.5	0.98	500	1.36	360	80	125.00
N-07-16	350	500	300	450	33.5	1.64	500	0.68	420	90	117.30
HS-33	254	508	215.9	469.9	28.34	1.33	321.99	1.28	328.88	104.9	63.3
HS-34	254	508	215.9	215.9	27.03	0.30	341.29	0.22	341.29	215.9	11.3
HS-35	254	508	215.9	215.9	26.54	0.39	334.4	0.41	344.74	117.6	15.3
HS-36	254	508	215.9	215.9	26.89	0.49	330.95	0.61	329.57	139.7	20
HS-37	254	508	215.9	215.9	27.17	0.59	336.46	0.86	327.5	98.6	25.3
HS-38	254	508	215.9	215.9	27.23	0.69	328.19	1.16	328.88	73.2	29.7
HS-39	254	508	215.9	215.9	27.58	0.79	315.78	1.57	327.5	54.1	34.2

Table A2. Weights of Hidden Layer of PCA.

j	i							Output
	1	2	3	4	5	6	Bias	
1	−0.1545	0.1662	0.1384	0.6391	0.4325	0.3042	0.9473	0.7981
2	−0.5281	1.1510	1.2343	0.2340	−0.4649	−0.6759	4.4658	−1.8626
3	−1.4639	0.1587	−0.4870	−0.0452	−0.2854	−0.3282	−0.7895	−1.5143
4	0.0019	0.0082	−0.0013	0.0156	0.0010	0.0044	−0.2514	0.0192
5	0.0020	0.0064	−0.0041	0.0183	0.0021	0.0068	−0.0726	0.0215
6	0.0029	0.0081	−0.0045	0.0209	0.0018	0.0083	−0.0249	0.0243
7	−0.0013	0.0037	−0.0012	0.0026	0.0005	0.0000	0.5251	0.0051
8	0.0009	0.0031	−0.0023	0.0062	0.0008	0.0028	−0.1684	0.0080
9	0.0041	0.0105	−0.0044	0.0232	0.0009	0.0087	−0.0521	0.0280
10	−0.1247	0.1927	−0.4994	−0.1091	−0.5657	−0.1735	0.9192	0.6379
11	−0.3498	0.0057	0.0178	−0.3881	0.0938	−0.9444	0.9381	−0.8587
12	−0.1445	−0.6899	−0.1118	−2.1050	0.5718	0.2138	0.9358	1.2367
13	0.0008	0.0045	−0.0031	0.0067	0.0005	0.0042	0.0629	0.0093
14	0.3453	−0.1055	1.0681	0.4641	−0.4305	0.3656	−0.4678	−0.7170
15	0.0038	0.0104	−0.0094	0.0407	0.0045	0.0165	0.1316	0.0450
16	0.0028	0.0051	−0.0024	0.0145	0.0003	0.0080	−0.3654	0.0145
17	0.0035	0.0091	−0.0060	0.0268	0.0027	0.0108	0.0385	0.0311

Table A2. *Cont.*

j	i							Output
	1	2	3	4	5	6	Bias	
18	−0.0006	0.0009	−0.0011	−0.0007	−0.0001	0.0006	0.0116	0.0012
19	0.0003	0.0031	−0.0021	0.0049	0.0002	0.0029	−0.0442	0.0076
20	−0.0020	−0.0016	0.0003	−0.0067	−0.0010	−0.0008	−0.2061	−0.0061
21	0.1284	−0.0049	−0.5827	0.6024	−0.7819	0.0078	0.0088	1.0035
22	1.0685	1.0795	−0.3224	−1.1641	0.0630	0.0932	−0.3027	−1.7037
23	0.0002	0.0020	−0.0022	0.0049	0.0003	0.0029	−0.2849	0.0053
24	0.0012	−0.0050	0.0057	−0.0036	0.0051	−0.0082	−1.1914	−0.0106
25	0.0033	0.0121	−0.0120	0.0516	0.0082	0.0197	0.1696	0.0578
26	0.7212	−0.7731	−0.2847	−0.9176	−0.3761	−0.7928	0.9476	1.0558
27	−0.0001	0.0011	−0.0021	0.0008	−0.0001	0.0016	0.1582	0.0024
28	0.0002	0.0005	−0.0012	−0.0025	−0.0005	−0.0004	0.1512	0.0001
29	−0.0082	−0.0771	0.0585	−0.1788	−0.0213	−0.0640	−0.4771	−0.2064
30	0.0036	−0.0264	0.0254	−0.0324	0.0005	−0.0274	−0.3046	−0.0596
31	−0.0009	0.0127	−0.0085	0.0164	0.0019	0.0168	0.1461	0.0278
32	−0.0013	−0.0016	0.0000	−0.0077	−0.0009	−0.0022	−0.0323	−0.0067
33	−0.0011	0.0001	−0.0017	−0.0011	−0.0003	0.0003	0.0040	−0.0002
34	−0.0021	−0.0002	−0.0014	−0.0059	−0.0001	−0.0041	0.3393	−0.0035
35	0.0031	0.0085	−0.0060	0.0270	0.0036	0.0110	0.0687	0.0312
36	0.0011	0.0035	−0.0034	0.0083	−0.0009	0.0038	−0.1523	0.0109
37	0.0005	0.0034	−0.0021	0.0157	0.0007	0.0056	−0.3042	0.0175
38	−0.2065	0.9972	−0.3582	−0.2333	−0.4763	0.3482	0.2780	1.0032
39	0.0003	0.0023	−0.0023	0.0055	0.0001	0.0024	−0.0375	0.0075
40	0.0035	0.0085	−0.0051	0.0199	0.0016	0.0086	0.1094	0.0239
41	0.0015	0.0050	−0.0034	0.0126	0.0011	0.0055	−0.1113	0.0147
42	−0.0098	−0.0442	0.0361	−0.1166	−0.0103	−0.0444	−0.4152	−0.1293
43	0.0003	0.0010	−0.0018	−0.0005	−0.0002	0.0009	0.2403	0.0025
44	−0.4171	−0.8559	0.4381	−0.3890	−0.6355	−0.0345	−1.6492	−1.1249
45	−0.0012	0.0000	−0.0008	−0.0062	−0.0005	−0.0015	0.2185	−0.0032
46	−0.0005	−0.0009	−0.0008	−0.0066	−0.0007	−0.0015	0.1369	−0.0040
47	−0.0017	−0.0124	−0.0028	−0.0220	−0.0022	0.0022	0.4295	−0.0091
48	0.0370	−0.0410	−0.1221	0.0599	−0.0004	0.1190	−1.7507	0.1534
49	0.1348	0.0679	0.0561	0.2256	0.0476	0.1361	0.6825	0.2366
50	0.0021	0.0057	−0.0036	0.0145	0.0007	0.0070	−0.0250	0.0174
51	1.3530	−1.6506	−1.2656	−0.6204	−0.1295	−0.3793	−2.6746	1.7284
52	0.0011	0.0037	−0.0022	0.0072	0.0004	0.0039	0.2319	0.0109

Table A3. Weights of Hidden Layer of Autoencoder.

											i											
j	**1**	**2**	**3**	**4**	**5**	**6**	**7**	**8**	**9**	**10**	**11**	**12**	**13**	**14**	**15**	**16**	**17**	**18**	**19**	**20**	**Bias**	**Output**
1	0.479	0.091	0.116	−0.027	−0.123	0.203	0.203	0.092	−0.194	−0.275	−0.128	0.309	−0.191	−1.096	0.062	−0.183	0.303	0.170	−0.236	−0.148	−1.762	−1.164
2	0.203	−0.587	−0.370	−0.223	−0.211	−0.076	0.282	−0.009	−0.108	−0.008	−0.043	−0.197	0.391	0.324	−0.061	0.418	0.349	−0.137	−0.095	0.066	0.331	−0.737
3	−0.007	0.010	0.017	−0.014	−0.014	0.019	0.010	−0.007	−0.034	−0.007	−0.001	−0.010	0.022	0.006	−0.002	0.016	0.009	−0.002	0.012	0.002	−0.559	0.061
4	0.013	−0.018	−0.037	0.024	0.028	−0.035	−0.022	0.016	0.066	0.016	0.005	0.017	−0.043	−0.015	0.006	−0.026	−0.019	0.004	−0.025	0.000	0.648	−0.119
5	0.000	0.009	−0.006	−0.011	−0.010	0.007	0.005	−0.004	−0.001	0.002	0.011	0.000	−0.007	−0.009	0.003	−0.007	0.005	0.008	−0.005	−0.006	0.118	0.014
6	0.005	−0.006	−0.010	0.008	0.010	−0.012	−0.008	0.004	0.023	0.004	−0.001	0.008	−0.015	0.000	0.000	−0.010	−0.007	0.002	−0.007	−0.003	0.186	−0.043
7	−0.237	0.032	−0.110	−0.051	0.215	0.305	−0.321	−0.083	0.010	−0.151	−0.166	−0.186	0.224	0.646	−0.117	0.564	−0.085	0.141	0.480	−0.178	−0.922	0.949
8	0.004	−0.005	−0.011	0.009	0.009	−0.012	−0.008	0.005	0.023	0.004	−0.001	0.008	−0.015	−0.001	0.000	−0.010	−0.007	0.002	−0.007	−0.003	0.210	−0.044
9	0.000	−0.004	0.002	0.004	0.006	−0.003	0.000	0.003	0.002	−0.002	−0.003	0.002	0.004	0.005	−0.005	0.000	0.000	−0.002	0.002	−0.002	0.293	−0.001
10	−0.077	−0.023	0.148	−0.024	−0.164	0.122	0.083	−0.054	−0.196	−0.124	0.000	−0.011	0.151	0.158	−0.131	0.028	0.119	0.024	0.075	−0.150	−1.517	0.484
11	−0.005	0.006	0.009	−0.008	−0.009	0.011	0.006	−0.005	−0.021	−0.004	0.000	−0.007	0.014	0.002	−0.001	0.010	0.006	−0.001	0.008	0.002	−0.448	0.036
12	0.005	−0.006	−0.012	0.006	0.007	−0.005	−0.004	−0.001	0.011	−0.002	0.006	0.001	−0.002	−0.008	0.004	−0.001	−0.002	−0.004	−0.005	−0.001	0.603	−0.024
13	1.183	0.053	0.276	−0.822	0.604	0.694	0.044	−0.155	0.124	−0.072	−0.005	0.319	0.463	0.277	−0.996	−0.213	0.141	0.456	−0.241	−0.073	−3.233	1.624
14	0.045	−0.179	0.543	0.259	−0.603	0.120	0.236	−0.131	−0.704	−0.315	0.105	0.066	0.279	0.098	−0.495	−0.071	0.136	0.156	0.423	−0.393	−3.889	1.460
15	−0.064	−0.019	−0.085	−0.032	−0.029	−0.194	−0.183	0.079	0.285	0.103	−0.094	0.094	−0.228	0.508	0.121	−0.159	−0.120	−0.071	0.026	−0.005	−0.927	−0.682
16	−0.005	−0.017	−0.020	0.024	0.024	−0.027	−0.015	0.013	0.058	0.006	0.017	0.034	−0.034	−0.020	−0.035	−0.016	−0.014	0.011	−0.024	−0.012	0.475	−0.093
17	0.000	0.000	0.000	0.001	0.000	−0.001	0.000	0.000	0.001	0.000	0.000	0.000	0.000	0.000	−0.001	0.001	0.000	0.000	0.000	−0.001	−0.090	−0.002
18	−0.115	−0.114	0.170	0.017	−0.336	0.175	0.105	−0.040	−0.219	−0.239	0.154	−0.017	0.165	0.145	−0.157	−0.022	0.190	0.038	0.003	−0.241	−1.526	0.678
19	0.503	0.336	0.428	−0.239	−0.106	0.081	0.008	−0.132	0.480	−0.175	−0.532	−0.482	−0.312	0.426	1.488	0.138	0.357	0.233	−0.479	−0.203	1.079	1.550
20	0.206	−0.164	−0.236	−0.047	0.006	−0.082	−0.037	0.207	0.378	−0.040	0.295	0.028	−0.224	−0.160	0.185	−0.092	−0.055	−0.017	−0.406	0.133	2.651	−0.893
21	0.010	−0.014	−0.025	0.019	0.021	−0.026	−0.015	0.011	0.049	0.010	0.001	0.014	−0.032	−0.007	0.003	−0.021	−0.014	0.003	−0.017	−0.003	0.522	−0.089
22	0.007	−0.008	−0.016	0.013	0.014	−0.017	−0.011	0.008	0.033	0.006	−0.001	0.011	−0.022	−0.003	0.001	−0.014	−0.009	0.003	−0.010	−0.003	0.361	−0.061
23	0.000	−0.002	−0.005	0.004	0.002	−0.003	−0.002	0.000	0.002	0.001	−0.002	0.000	−0.002	0.003	0.002	−0.004	−0.001	−0.001	0.000	−0.002	−0.654	−0.010
24	0.292	0.134	0.269	−0.123	−0.105	−0.198	0.262	−0.092	0.598	0.188	−0.447	−0.292	−0.404	0.488	0.882	0.172	−0.359	0.154	−0.278	0.061	−0.230	−1.305

References

1. ACI Committee. *Building Code Requirements for Structural Concrete (ACI 318-19) and Commentary*; American Concrete Institute: Indianapolis, IN, USA, 2019.
2. EC2. *Eurocode 2: Design of Concrete Structures: Part 1-1: General Rules and Rules for Buildings*; British Standards Institution: London, UK, 2004.
3. CSA A23. *3-14. CSA A23. 3-14: Design of Concrete Structures*; Canadian Medical Association Journal: Toronto, ON, Canada, 2014.
4. JSCE. *Standard Specifications for Concrete Structures*; Japan Society of Civil Engineers: Shinjuku, Tokyo, 2007.
5. Rausch, E. Design of Reinforced Concrete in Torsion (Berechnung des Eisenbetons Gegen Verdrehung). Ph.D. Thesis, Technische Hochschule, Berlin, Germany, 1929; p. 53. (In German)
6. Bredt, R. Kritische Bemerkungen Zur Drehungselastizitat. *Zeitschrift des Vereines Dtsch. Ingenieure* **1896**, *40*, 785–790.
7. Hsu, T.T.C. Shear Flow Zone in Torsion of Reinforced Concrete. *J. Struct. Eng.* **1990**, *116*, 3206–3226. [CrossRef]
8. Jeng, C.H.; Hsu, T.T.C. A Softened Membrane Model for Torsion in Reinforced Concrete Members. *Eng. Struct.* **2009**, *31*, 1944–1954. [CrossRef]
9. Hsu, T.T.C. Torsion of Structural Concrete-Behavior of Reinforced Concrete Rectangular Members. *Spec. Publ.* **1968**, *18*, 261–306.
10. Victor, D.J.; Muthukrishnan, R. Effect of Stirrups on Ultimate Torque of Reinforced Concrete Beams. *J. Proc.* **1973**, *70*, 300–306.
11. McMullen, A.E.; Rangan, B.V. Pure Tension in Rectangular Sections-A Re-Examination. *J. Proc.* **1978**, *75*, 511–519.
12. Collins, M.P.; Mitchell, D. Shear and Torsion Design of Prestressed and Non Prestressed Concrete Beams. *Prestress. Concr. Inst. (PCI) J. USA* **1980**, *25*, 32–100. [CrossRef]
13. Hsu, T.T.C.; Mo, Y.L. Softening of Concrete in Torsional Members-Theroy and Tests. *J. Proc.* **1985**, *82*, 290–303.
14. Koutchoukali, N.-E.; Belarbi, A. Torsion of High-Strength Reinforced Concrete Beams and Minimum Reinforcement Requirement. *Struct. J.* **2001**, *98*, 462–469.
15. Fang, I.-K.; Shiau, J.-K. Torsional Behavior of Normal-and High-Strength Concrete Beams. *Struct. J.* **2004**, *101*, 304–313.
16. Chiu, H.J.; Fang, I.K.; Young, W.T.; Shiau, J.K. Behavior of Reinforced Concrete Beams with Minimum Torsional Reinforcement. *Eng. Struct.* **2007**, *29*, 2193–2205. [CrossRef]
17. Bernardo, L.F.A.; Lopes, S.M.R. Torsion in High-Strength Concrete Hollow Beams: Strength and Ductility Analysis. *ACI Struct. J.* **2009**, *106*, 39–48.
18. Yang, I.H.; Joh, C.; Lee, J.W.; Kim, B.S. Torsional Behavior of Ultra-High Performance Concrete Squared Beams. *Eng. Struct.* **2013**, *56*, 372–383. [CrossRef]
19. Chalioris, C.E. Experimental Study of the Torsion of Reinforced Concrete Members. *Struct. Eng. Mech.* **2006**, *23*, 713–737. [CrossRef]
20. Chalioris, C.E.; Karayannis, C.G. Experimental Investigation of RC Beams with Rectangular Spiral Reinforcement in Torsion. *Eng. Struct.* **2013**, *56*, 286–297. [CrossRef]
21. Hassan, A.; Hafez, L.A. Investigation of Torsional Behaviour of High-Strength Reinforced Concrete Sections. *World Appl. Sci. J.* **2015**, *33*, 1–13. [CrossRef]
22. Lee, J.; Kim, K.; Lee, S.H.; Kim, C.; Kim, M. Maximum Torsional Reinforcement of Reinforced Concrete Beams Subjected to Pure Torsion. *ACI Struct. J.* **2018**, *115*, 749–761. [CrossRef]
23. Sanad, A.; Saka, M.P. Prediction of Ultimate Shear Strength of Reinforced-Concrete Deep Beams Using Neural Networks. *J. Struct. Eng.* **2001**, *127*, 818–828. [CrossRef]
24. Adhikary, B.B.; Mutsuyoshi, H. Artificial Neural Networks for the Prediction of Shear Capacity of Steel Plate Strengthened RC Beams. *Constr. Build. Mater.* **2004**, *18*, 409–417. [CrossRef]
25. Cladera, A.; Marí, A.R. Shear Design Procedure for Reinforced Normal and High-Strength Concrete Beams Using Artificial Neural Networks. Part II: Beams with Stirrups. *Eng. Struct.* **2004**, *26*, 927–936. [CrossRef]
26. Mansour, M.Y.; Dicleli, M.; Lee, J.Y.; Zhang, J. Predicting the Shear Strength of Reinforced Concrete Beams Using Artificial Neural Networks. *Eng. Struct.* **2004**, *26*, 781–799. [CrossRef]
27. Oreta, A.W.C. Simulating Size Effect on Shear Strength of RC Beams without Stirrups Using Neural Networks. *Eng. Struct.* **2004**, *26*, 681–691. [CrossRef]
28. Adhikary, B.B.; Mutsuyoshi, H. Prediction of Shear Strength of Steel Fiber RC Beams Using Neural Networks. *Constr. Build. Mater.* **2006**, *20*, 801–811. [CrossRef]
29. Abdalla, J.A.; Elsanosi, A.; Abdelwahab, A. Modeling and Simulation of Shear Resistance of R/C Beams Using Artificial Neural Network. *J. Franklin Inst.* **2007**, *344*, 741–756. [CrossRef]
30. Yang, K.; Ashour, A.F.; Song, J. Shear Capacity of Reinforced Concrete Beams Using Neural Network. *Int. J. Concr. Struct. Mater.* **2007**, *1*, 63–73. [CrossRef]
31. Perera, R.; Barchín, M.; Arteaga, A.; Diego, A.D. Prediction of the Ultimate Strength of Reinforced Concrete Beams FRP-Strengthened in Shear Using Neural Networks. *Compos. Part B Eng.* **2010**, *41*, 287–298. [CrossRef]
32. Tanarslan, H.M.; Secer, M.; Kumanlioglu, A. An Approach for Estimating the Capacity of RC Beams Strengthened in Shear with FRP Reinforcements Using Artificial Neural Networks. *Constr. Build. Mater.* **2012**, *30*, 556–568. [CrossRef]

33. Tang, C.-W. Using Radial Basis Function Neural Networks to Model Torsional Strength of Reinforced Concrete Beams. *Comput. Concr.* **2006**, *3*, 335–355. [CrossRef]
34. Cevik, A.; Arslan, M.H.; Köroğlu, M.A. Genetic-Programming-Based Modeling of RC Beam Torsional Strength. *KSCE J. Civ. Eng.* **2010**, *14*, 371–384. [CrossRef]
35. Arslan, M.H. Predicting of Torsional Strength of RC Beams by Using Different Artificial Neural Network Algorithms and Building Codes. *Adv. Eng. Softw.* **2010**, *41*, 946–955. [CrossRef]
36. Witten, I.H.; Frank, E.; Hall, M.A.; Pal, C.J. *Data Mining: Practical Machine Learning Tools and Techniques*; Morgan Kaufmann Publishers: Burlington, MA, USA, 2016.
37. Kim, C.; Lee, J.-Y.; Kim, M. Prediction of the Dynamic Stiffness of Resilient Materials Using Artificial Neural Network (ANN) Technique. *Appl. Sci.* **2019**, *9*, 1088. [CrossRef]
38. Alwattar, T.A.; Mian, A. Development of an Elastic Material Model for BCC Lattice Cell Structures Using Finite Element Analysis and Neural Networks Approaches. *J. Compos. Sci.* **2019**, *3*, 33. [CrossRef]
39. Al-Wattar, T.A.A. Developing Equivalent Solid Model for Lattice Cell Structure Using Numerical Approaches. Ph.D. Thesis, Wright State University, Dayton, OH, USA, 2020.
40. Rasmussen, L.J.; Baker, G. Torsion in Reinforced Normal and High-Strength Concrete Beams Part 1: Experimental Test Series. *Struct. J.* **1995**, *92*, 56–62.
41. Rahal, K.N.; Collins, M.P. Simple Model for Predicting Torsional Strength of Reinforced and Pre-Stressed Concrete Sections. *ACI Struct. J.* **1996**, *93*, 658–666.
42. Kim, C.; Kim, S.; Kim, K.; Shin, D.; Haroon, M.; Lee, J. Torsional Behavior of Reinforced Concrete Beams with High-Strength Steel Bars. *ACI Struct. J.* **2019**, *116*, 251–263. [CrossRef]
43. Lee, J.-Y.; Kim, S.-W. Torsional Strength of RC Beams Considering Tension Stiffening Effect. *J. Struct. Eng.* **2010**, *136*, 1367–1378. [CrossRef]
44. Campbell, N.A.; Atchley, W.R. The Geometry of Canonical Variate Analysis. *Syst. Biol.* **1981**, *30*, 268–280. [CrossRef]
45. Freedman, D.; Pisani, R.; Purves, R.; Adhikari, A. *Statistics*, 2nd ed.; WW Norton: New York, NY, USA, 1991.
46. Liou, C.-Y.; Cheng, W.-C.; Liou, J.-W.; Liou, D.-R. Autoencoder for Words. *Neurocomputing* **2014**, *139*, 84–96. [CrossRef]
47. Zhang, L.; Ma, W.; Zhang, D. Stacked Sparse Autoencoder in PolSAR Data Classification Using Local Spatial Information. *IEEE Geosci. Remote Sens. Lett.* **2016**, *13*, 1359–1363. [CrossRef]
48. Shao, Z.; Zhang, L.; Wang, L. Stacked Sparse Autoencoder Modeling Using the Synergy of Airborne LiDAR and Satellite Optical and SAR Data to Map Forest Above-Ground Biomass. *IEEE J. Sel. Top. Appl. Earth Obs. Remote Sens.* **2017**, *10*, 5569–5582. [CrossRef]
49. Ayinde, B.O.; Zurada, J.M. Deep Learning of Constrained Autoencoders for Enhanced Understanding of Data. *IEEE Trans. Neural Networks Learn. Syst.* **2017**, *29*, 3969–3979. [CrossRef]
50. Poultney, C.; Chopra, S.; Cun, Y.L. Efficient Learning of Sparse Representations with an Energy-Based Model. In *Advances in Neural Information Processing Systems*; Neural Information Processing Systems Foundation: San Diego, CA, USA, 2007; pp. 1137–1144.